

# Universal dynamics in the onset of a Hagen–Poiseuille flow

Niels Asger Mortensen and Henrik Bruus

*MIC – Department of Micro and Nanotechnology, NanoDTU,  
Technical University of Denmark, DK-2800 Kongens Lyngby, Denmark*

(Dated: January 17, 2006)

The dynamics in the onset of a Hagen–Poiseuille flow of an incompressible liquid in a channel of circular cross section is well-studied theoretically. We use an eigenfunction expansion in a Hilbert space formalism to generalize the results to channels of arbitrary cross section. We find that the steady state is reached after a characteristic time scale  $\tau = (\mathcal{A}/\mathcal{P})^2(1/\nu)$  where  $\mathcal{A}$  and  $\mathcal{P}$  are the cross-sectional area and perimeter, respectively, and  $\nu$  is the kinematic viscosity of the liquid. For the initial dynamics of the flow rate  $Q$  for  $t \ll \tau$  we find a universal linear dependence,  $Q(t) = Q_\infty (\alpha/\mathcal{C}) (t/\tau)$ , where  $Q_\infty$  is the asymptotic steady-state flow rate,  $\alpha$  is the geometrical correction factor, and  $\mathcal{C} = \mathcal{P}^2/\mathcal{A}$  is the compactness parameter. For the long-time dynamics  $Q(t)$  approaches  $Q_\infty$  exponentially on the timescale  $\tau$ , but with a weakly geometry-dependent prefactor of order unity, determined by the lowest eigenvalue of the Helmholtz equation.

PACS numbers: 47.10.A-, 47.15.Rq, 47.27.nd, 47.27.nf, 47.61.-k, 47.85.L-

## I. INTRODUCTION

Hagen–Poiseuille flow (or simply Poiseuille flow) is important to a variety of applications ranging from macroscopic pipes in chemical plants to the flow of blood in veins. However, the rapid development in the field of lab-on-a-chip systems during the past decade has put even more emphasis on pressure driven laminar flow. Traditionally, capillary tubes would have circular cross-sections, but today microfabricated channels come with a variety of shapes depending on the fabrication technique in use. The list of examples includes rectangular channels obtained by hot embossing in polymer wafers, semi-circular channels in isotropically etched surfaces, triangular channels in KOH-etched silicon crystals, Gaussian-shaped channels in laser-ablated polymer films, and elliptic channels in stretched PDMS devices, see e.g. Ref. 1.

This development has naturally led to more emphasis on theoretical studies of shape-dependence in microfluidic channels. Recently, we therefore revisited the problem of Poiseuille flow and its shape dependence and we have also addressed mass diffusion in microchannels [2, 3]. In the present work we combine the two former studies and address the dynamics caused by the abrupt onset of a pressure gradient at time  $t = 0$  in an incompressible liquid of viscosity  $\eta$  and density  $\rho$  situated in a long, straight, and rigid channel of length  $L$  and some constant cross-sectional shape  $\Omega$ . The solution is well-known for the case of a cylindrical channel, see e.g. Ref. 4, but in this paper we generalize the results to a cross-section of arbitrary shape. The similarity between mass and momentum diffusion, and the existence of a characteristic diffusion time-scale  $\tau_{\text{diff}} = (\pi/4)(\mathcal{A}/\mathcal{P})^2/D$  for mass diffusion [3] have led us to introduce the momentum diffusion time-scale  $\tau$  defined by

$$\tau = \left(\frac{\mathcal{A}}{\mathcal{P}}\right)^2 \frac{1}{\nu}, \quad (1)$$

where  $\nu = \eta/\rho$  is the kinematic viscosity (having dimen-

sions of a diffusion constant), while  $\mathcal{A}$  and  $\mathcal{P}$  is the area and perimeter of the cross section  $\Omega$ , respectively. In this paper we show that the dynamics of the flow rate  $Q(t)$  is universal with  $\tau$  as the characteristic time scale.

As shown in Ref. 2 the shape parameters  $\mathcal{A}$  and  $\mathcal{P}$  also play an important role in the steady-state Poiseuille flow. The hydraulic resistance  $R_{\text{hyd}}$  can be expressed as

$$R_{\text{hyd}} = \alpha \frac{\eta L}{\mathcal{A}^2} \equiv \alpha R_{\text{hyd}}^*, \quad (2)$$

where  $\alpha$  is a dimensionless geometrical correction factor and  $R_{\text{hyd}}^* = \eta L/\mathcal{A}^2$  is a characteristic resistance. Remarkably,  $\alpha$  is simply (linearly) related to the dimensionless compactness parameter  $\mathcal{C} = \mathcal{P}^2/\mathcal{A}$ .

Above we have emphasized microfluidic flows because of the variety of shapes frequently encountered in lab-on-a-chip systems. However, our results are generally valid for laminar flows at any length scale.

## II. DIFFUSION OF MOMENTUM

We consider a long, straight channel of length  $L$ , aligned with the  $z$ -axis, having a constant cross section  $\Omega$  with the boundary  $\partial\Omega$  in the  $xy$  plane. The fluid flow is driven by a pressure gradient of  $\nabla p = -(\Delta p/L)\mathbf{e}_x$  which is turned on abruptly at time  $t = 0$ . We note that strictly speaking the pressure gradient is not established instantaneously, but rather on a time-scale set by  $L/c$  where  $c$  is the speed of sound. For typical liquids  $c \sim 10^3$  m/s which for micro-fluidic systems and practical purposes makes the pressure gradient appear almost instantaneously. From the symmetry of the problem it follows that the velocity field is of the form  $\mathbf{v}(\mathbf{r}, t) = v(\mathbf{r}_\perp, t)\mathbf{e}_x$  where  $\mathbf{r}_\perp = y\mathbf{e}_y + z\mathbf{e}_z$ . From the Navier–Stokes equation it then follows that  $v(\mathbf{r}_\perp, t)$  is governed by, see e.g. Refs. 4 or 5,

$$\frac{1}{\nu} \partial_t v(\mathbf{r}_\perp, t) - \nabla^2 v(\mathbf{r}_\perp, t) = \frac{\Delta p}{\eta L}, \quad (3)$$

which is a diffusion equation for the momentum with the pressure drop acting as a source term on the right-hand side. The velocity  $v$  is subject to a no-slip boundary condition on  $\partial\Omega$  and obviously  $v$  is initially zero, while it asymptotically approaches the steady-state velocity field  $v_\infty(\mathbf{r}_\perp)$  for  $t \rightarrow \infty$ .

In the analysis it is natural to write the velocity as a difference

$$v(\mathbf{r}_\perp, t) = v_\infty(\mathbf{r}_\perp) - v_h(\mathbf{r}_\perp, t) \quad (4)$$

of the asymptotic, static field  $v_\infty$ , solving the Poiseuille problem

$$-\nabla^2 v_\infty(\mathbf{r}_\perp) = \frac{\Delta p}{\eta L}, \quad (5)$$

and a time-dependent field  $v_h(\mathbf{r}_\perp, t)$  satisfying the homogeneous diffusion equation,

$$\frac{1}{\nu} \partial_t v_h(\mathbf{r}_\perp, t) - \nabla^2 v_h(\mathbf{r}_\perp, t) = 0. \quad (6)$$

From Ref. 3 it is known that rescaling the Helmholtz equation by  $(\mathcal{A}/\mathcal{P})^2$  leads to a lowest eigenvalue  $a_1$  that is of order unity and only weakly geometry dependent. We therefore perform this rescaling, which naturally implies the time-scale  $\tau$  of Eq. (1) and the following form of the diffusion equation,

$$\tau \partial_t v_h(\mathbf{r}_\perp, t) - \hat{\mathcal{L}} v_h(\mathbf{r}_\perp, t) = 0. \quad (7)$$

where we have introduced the rescaled Laplacian  $\hat{\mathcal{L}}$ ,

$$\hat{\mathcal{L}} \equiv \left(\frac{\mathcal{A}}{\mathcal{P}}\right)^2 \nabla^2. \quad (8)$$

We note that by the rescaling the Navier–Stokes equation (3) becomes

$$\tau \partial_t v - \hat{\mathcal{L}} v = \left(\frac{\mathcal{A}}{\mathcal{P}}\right)^2 \frac{\Delta p}{\eta L} = \frac{\alpha Q_\infty}{\mathcal{P}^2}, \quad (9)$$

where we have introduced the steady-state flow rate  $Q_\infty = \Delta p/R_{\text{hyd}}$  and used Eq. (2).

### III. HILBERT SPACE FORMULATION

In order to solve Eq. (9) we will take advantage of the Hilbert space formulation [6], often employed in quantum mechanics [7]. The Hilbert space of real functions  $f(\mathbf{r}_\perp)$  is defined by the inner product

$$\langle f|g \rangle \equiv \int_\Omega d\mathbf{r}_\perp f(\mathbf{r}_\perp)g(\mathbf{r}_\perp) \quad (10)$$

and a complete set  $\{|\phi_n\rangle\}$  of orthonormal basis functions,

$$\langle \phi_m|\phi_n \rangle = \delta_{nm}. \quad (11)$$

Above, we have used the Dirac *bra-ket* notation and  $\delta_{nm}$  is the Kronecker delta. We choose the eigenfunctions  $\{|\phi_n\rangle\}$  of the rescaled Helmholtz equation (with a zero Dirichlet boundary condition on  $\partial\Omega$ ) as our basis functions,

$$-\hat{\mathcal{L}}|\phi_n\rangle = a_n|\phi_n\rangle. \quad (12)$$

With this complete basis any function in the Hilbert space can be written as a linear combination of basis functions. Using the *bra-ket* notation Eq. (9) becomes

$$\tau \partial_t |v\rangle - \hat{\mathcal{L}}|v\rangle = \frac{\alpha Q_\infty}{\mathcal{P}^2}|1\rangle. \quad (13)$$

The full solution Eq. (4) is written as

$$|v\rangle = |v_\infty\rangle - |v_h\rangle, \quad (14)$$

where  $|v_\infty\rangle$  satisfies the Poiseuille problem Eq. (5),

$$-\hat{\mathcal{L}}|v_\infty\rangle = \frac{\alpha Q_\infty}{\mathcal{P}^2}|1\rangle, \quad (15)$$

and the homogeneous solution  $|v_h\rangle$  solves the diffusion problem Eq. (7)

$$(\tau \partial_t - \hat{\mathcal{L}})|v_h\rangle = 0. \quad (16)$$

In the complete basis  $\{|\phi_n\rangle\}$  we have

$$|v_h\rangle = \sum_{n=1}^{\infty} b_n e^{-a_n t/\tau} |\phi_n\rangle, \quad (17)$$

$$|v_\infty\rangle = \sum_{n=1}^{\infty} c_n |\phi_n\rangle, \quad (18)$$

and since  $\lim_{t \rightarrow 0} |v_h\rangle = |v_\infty\rangle$  we have  $b_n = c_n$ . Multiplying Eq. (18) by  $\langle \phi_m|$  yields

$$\begin{aligned} b_m = c_m &= \langle \phi_m|v_\infty\rangle = \langle \phi_m|\hat{\mathcal{L}}^{-1}\hat{\mathcal{L}}|v_\infty\rangle \\ &= \frac{\alpha Q_\infty}{\mathcal{P}^2} a_m^{-1} \langle \phi_m|1\rangle. \end{aligned} \quad (19)$$

In the second-last equality we have introduced the unit operator  $1 = \hat{\mathcal{L}}^{-1}\hat{\mathcal{L}}$  and in the last equality we used the Hermitian property of the inverse Laplacian operator to let  $\hat{\mathcal{L}}^{-1}$  act to the left,  $\langle \phi_m|\hat{\mathcal{L}}^{-1} = -\langle \phi_m|a_m^{-1}$  from Eq. (12), while  $\hat{\mathcal{L}}$  acts to the right, see Eq. (15). Substituting Eqs. (17) and (19) into Eq. (14) we finally obtain

$$|v\rangle = |v_\infty\rangle - \frac{\alpha Q_\infty}{\mathcal{P}^2} \sum_{n=1}^{\infty} |\phi_n\rangle \langle \phi_n|1\rangle a_n^{-1} e^{-a_n t/\tau}. \quad (20)$$

### IV. FLOW RATE

Using the *bra-ket* notation, the flow rate  $Q(t)$  at any time is conveniently written as  $Q = \langle 1|v\rangle$ , and thus in

steady state  $Q_\infty = \langle 1|v_\infty\rangle$ . Multiplying Eq. (20) from the left by  $\langle 1|$  yields

$$Q(t) = \langle 1|v\rangle = Q_\infty - \frac{\alpha Q_\infty}{\mathcal{P}^2} \sum_{n=1}^{\infty} \langle 1|\phi_n\rangle \langle \phi_n|1\rangle a_n^{-1} e^{-a_n t/\tau}. \quad (21)$$

The factor  $\langle 1|\phi_n\rangle \langle \phi_n|1\rangle$  is recognized as the effective area  $\mathcal{A}_n$  covered by the  $n$ th eigenfunction  $|\phi_n\rangle$ ,

$$\mathcal{A}_n \equiv \frac{|\langle 1|\phi_n\rangle|^2}{\langle \phi_n|\phi_n\rangle} = |\langle 1|\phi_n\rangle|^2 = \langle 1|\phi_n\rangle \langle \phi_n|1\rangle. \quad (22)$$

The effective areas fulfil the sum-rule  $\sum_{n=1}^{\infty} \mathcal{A}_n = \mathcal{A}$ , seen by completeness of the basis  $\{|\phi_n\rangle\}$ . We can find the geometrical correction factor  $\alpha$  from Eq. (21) by using that  $Q(0) = 0$ ,

$$\alpha = \mathcal{P}^2 \left( \sum_{n=1}^{\infty} \frac{\mathcal{A}_n}{a_n} \right)^{-1}, \quad (23)$$

and substituting into Eq. (21) we finally get

$$\frac{Q(t)}{Q_\infty} = 1 - \left( \sum_{n=1}^{\infty} \frac{\mathcal{A}_n}{a_n} \right)^{-1} \sum_{n=1}^{\infty} \frac{\mathcal{A}_n}{a_n} e^{-a_n t/\tau}. \quad (24)$$

## V. SHORT-TIME DYNAMICS

The short-time dynamics is found by Taylor-expanding Eq. (24) to first order,

$$\frac{Q(t)}{Q_\infty} \approx \left( \sum_{n=1}^{\infty} \frac{\mathcal{A}_n}{a_n} \right)^{-1} \mathcal{A} \frac{t}{\tau} = \frac{\alpha \mathcal{A}}{\mathcal{P}^2} \frac{t}{\tau} = \frac{\alpha}{\mathcal{C}} \frac{t}{\tau}, \quad t \ll \tau, \quad (25)$$

where we have used the sum-rule for  $\mathcal{A}_n$  as well as Eq. (23). The short time dynamics can also be inferred directly by integration of the Navier–Stokes equation Eq. (13), since at time  $t = 0$  we have  $|v\rangle = 0$  and consequently the vanishing of velocity gradients and viscous friction,  $\mathcal{L}|v\rangle = 0$ . Thus we arrive at

$$\tau \partial_t |v\rangle = \frac{\alpha Q_\infty}{\mathcal{P}^2} |1\rangle, \quad t \rightarrow 0, \quad (26)$$

corresponding to a constant initial acceleration throughout the fluid. Integration with respect to  $t$  is straightforward and multiplying the resulting  $|v\rangle$  by  $\langle 1|$  yields  $Q(t)$ ,

$$\frac{Q(t)}{Q_\infty} \simeq \frac{\alpha}{\mathcal{P}^2} \langle 1|1\rangle \frac{t}{\tau} = \frac{\alpha \mathcal{A}}{\mathcal{P}^2} \frac{t}{\tau} = \frac{\alpha}{\mathcal{C}} \frac{t}{\tau}, \quad t \ll \tau. \quad (27)$$

Thus initially, the fluid responds to the pressure gradient in the same way as a rigid body responds to a constant force.

shape	$a_1$	$\mathcal{A}_1/\mathcal{A}$	$\alpha/\mathcal{C}$
circle	$\gamma_{0,1}^2/4 \simeq 1.45^a$	$4/\gamma_{0,1}^2 \simeq 0.69^a$	$2^b$
quarter-circle	$1.27^c$	$0.65^c$	$1.85^c$
half-circle	$1.38^c$	$0.64^c$	$1.97^c$
ellipse(1:2)	$1.50^c$	$0.67^c$	$2.10^c$
ellipse(1:3)	$1.54^c$	$0.62^c$	$2.21^c$
ellipse(1:4)	$1.57^c$	$0.58^c$	$2.28^c$
triangle(1:1:1)	$\pi^2/9 \simeq 1.10^d$	$6/\pi^2 \simeq 0.61^d$	$5/3^b$
triangle(1:1: $\sqrt{2}$ )	$\frac{5\pi^2}{4(2+\sqrt{2})^2} \simeq 1.06^a$	$512/9\pi^4 \simeq 0.58^a$	$1.64^c$
square	$\pi^2/8 \simeq 1.23^a$	$64/\pi^4 \simeq 0.66^a$	$1.78^c$
rectangle(1:2)	$5\pi^2/36 \simeq 1.37^a$	$64/\pi^4 \simeq 0.66^a$	$1.94^c$
rectangle(1:3)	$5\pi^2/32 \simeq 1.54^a$	$64/\pi^4 \simeq 0.66^a$	$2.14^c$
rectangle(1:4)	$17\pi^2/100 \simeq 1.68^a$	$64/\pi^4 \simeq 0.66^a$	$2.28^c$
rectangle(1: $\infty$ )	$\sim \pi^2/4 \simeq 2.47^a$	$64/\pi^4 \simeq 0.66^a$	$\sim 3^e$
pentagon	$1.30^c$	$0.67^c$	$1.84^c$
hexagon	$1.34^c$	$0.68^c$	$1.88^c$

TABLE I: Central parameters for the lowest eigenfunction for different cross sectional shapes. Note how the different numbers converge when going through the regular polygons starting from the triangle(1:1:1) through the square, the pentagon, and the hexagon to the circle. <sup>a</sup>See e.g. Ref. 6 for the eigenmodes and eigenspectrum. Here,  $\gamma_{0,1}$  denotes the first root of the zeroth Bessel function of the first kind. <sup>b</sup>See Ref. 2. <sup>c</sup>Data obtained by finite-element simulations. <sup>d</sup>See e.g. Ref. 8 for the eigenmodes and eigenspectrum. <sup>e</sup>See e.g. Ref. 4 for a solution of the Poisson equation.

## VI. LONG-TIME DYNAMICS

As the flow rate increases, friction sets in, and in the long-time limit  $t \gg \tau$  the flow-rate saturates at the value  $Q_\infty$  where there is a balance between the pressure gradient and frictional forces. For the long-time saturation dynamics the lowest eigenstate plays the dominating role and taking only the  $n = 1$  term in Eq. (24) we obtain

$$\frac{Q(t)}{Q_\infty} \simeq 1 - e^{-a_1 t/\tau}, \quad t \gg \tau/a_2, \quad (28)$$

where we have used that the lowest eigenvalue  $a_1$  is non-degenerate to truncate the summation.

The time it takes to reach steady-state is denoted  $\tau_\infty$ . A lower bound  $\tau_1$  for  $\tau_\infty$  can be obtained from Eq. (27) by assuming that the initial acceleration is maintained until  $Q(\tau_1)/Q_\infty = 1$  is reached,

$$\tau_\infty > \tau_1 = \frac{\mathcal{C}}{\alpha} \tau. \quad (29)$$

A better estimate  $\tau_2$  for  $\tau_\infty$  is obtained from Eq. (28) by demanding  $Q(\tau_2)/Q_\infty = 1 - e^{-3}$ .

$$\tau_\infty \approx \tau_2 = \frac{3}{a_1} \tau. \quad (30)$$

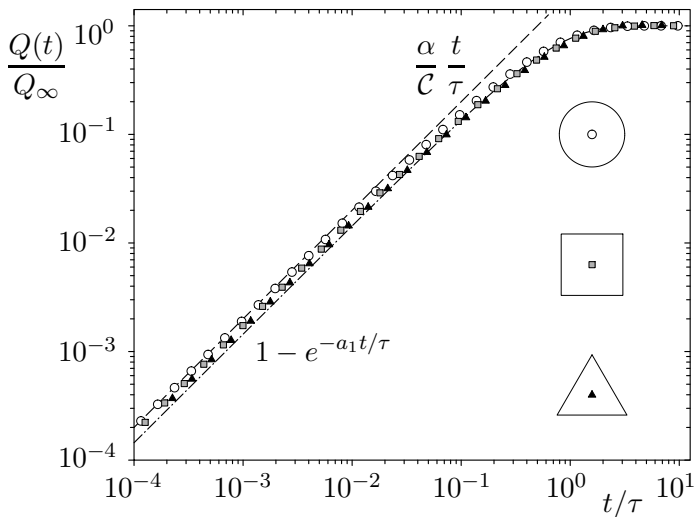


FIG. 1: A log-log plot of the flow rate  $Q(t)/Q_\infty$  as a function of time  $t/\tau$ . The dashed line is the short-time approximation Eq. (27), while the dashed-dotted line is the long-time approximation Eq. (28), both for the case of a circle, i.e., using  $\mathcal{C}/\alpha = 2$  and  $a_1 = 1.45$  as listed in Table I. The data points are the results of time-dependent finite-element simulations for the cases of the cross section being a circle (white circles), a square (gray squares), and an equilateral triangle (black triangles).

Using the parameter values for the circle listed in Table I we find the values

$$\tau_1 = 0.5 \tau < \tau_2 = 2.1 \tau \approx \tau_\infty. \quad (31)$$

## VII. NUMERICAL RESULTS

Only few geometries allow analytical solutions of both the Helmholtz equation and the Poisson equation. The circle is of course the most well-known example, but the equilateral triangle is another exception. How-

ever, in general the equations have to be solved numerically, and for this purpose we have used the commercially available finite-element software Comsol 3.2 (see [www.comsol.com](http://www.comsol.com)). Numbers for a selection of geometries are tabulated in Table I.

The circle is the most compact shape and consequently it has the largest value for  $\mathcal{A}_1/\mathcal{A}$ , i.e., the mode has the relatively largest spatial occupation of the total area. The eigenvalue  $a_1$  is of the order unity for compact shapes and in general it tends to increase slightly with increasing values of  $\mathcal{C}$ . The modest variation from geometry to geometry in both  $a_1$  and the other parameters suggests that the dynamics of  $Q(t)$  will appear almost universal.

In order to illustrate the validity of our two asymptotic expressions, Eqs. (27) and (28), we have compared them using the values for a circular shape to time-dependent finite-element simulations of Eq. (3). As illustrated in Fig. 1 we find a perfect agreement between the asymptotic expressions Eqs. (27) and (28) and the numerically exact data for a circle, a square, and an equilateral triangle. Comparing the corresponding parameters in Table I we would expect all data to almost coincide, which is indeed also observed in Fig. 1. The small spread in eigenvalues and other parameters thus gives rise to close-to-universal dynamics. From the plot it is also clear that  $\tau$  is indeed a good estimate for the time it takes to reach the steady state.

## VIII. CONCLUSIONS

In conclusion, by using a compact Hilbert space formalism we have shown how the initial dynamics in the onset of Poiseuille flow is governed by a universal linear raise in flow rate  $Q(t)$  over a universal time-scale  $\tau$  above which it saturates exponentially to the steady-state value  $Q_\infty$ . The steady state is reached after a time  $\tau_\infty \approx \mathcal{C}\tau/\alpha$ . Apart from being a fascinating example of universal dynamics for a complex problem our results may have important applications in design of real-time programmable pressure-driven micro-fluidic networks.

- 
- [1] O. Geschke, H. Klank, and P. Telleman, editors, *Microsystem Engineering of Lab-on-a-Chip Devices*, Wiley-VCH Verlag, Weinheim, 2004.
- [2] N. A. Mortensen, F. Okkels, and H. Bruus, *Phys. Rev. E* **71**, 057301 (2005).
- [3] N. A. Mortensen, F. Okkels, and H. Bruus, *Phys. Rev. E* **73**, 012101 (2006).
- [4] G. K. Batchelor, *An Introduction to Fluid Dynamics*, Cambridge University Press, Cambridge, 1967.
- [5] L. D. Landau and E. M. Lifshitz, *Fluid Mechanics*, volume 6 of *Landau and Lifshitz, Course of Theoretical Physics*, Butterworth-Heinemann, Oxford, 2nd edition, 1987.
- [6] P. M. Morse and H. Feshbach, *Methods of Theoretical Physics*, McGraw-Hill, New York, 1953.
- [7] E. Merzbacher, *Quantum Mechanics*, Wiley & Sons, New York, 1970.
- [8] M. Brack and R. K. Bhaduri, *Semiclassical Physics*, Addison Wesley, New York, 1997.